Author/s:
Zeng, P;Ren, X;Wei, L;Zhao, H;Liu, X;Zhang, X;Xu, Y;Yan, L;Boldt, K;Smith, TA;Liu, M

Title:
Control of Hot Carrier Relaxation in CsPbBr₃ Nanocrystals Using Damping Ligands

Date:
2022-04-04

Citation:
Zeng, P., Ren, X., Wei, L., Zhao, H., Liu, X., Zhang, X., Xu, Y., Yan, L., Boldt, K., Smith, T. A. & Liu, M. (2022). Control of Hot Carrier Relaxation in CsPbBr₃ Nanocrystals Using Damping Ligands. Angewandte Chemie, 134 (15), https://doi.org/10.1002/ange.202111443.

Author Manuscript

Title: Control of Hot Carrier Relaxation in CsPbBr3 Nanocrystals Using Damping Ligands

Authors: Peng Zeng, Ph.D; Xinjian Ren; Linfeng Wei; Haifeng Zhao; Xiaochun Liu; Xinyang Zhang; Yanmin Xu; Lihe Yan; Klaus Boldt; Trevor A. Smith; Mingzhen Liu

To be cited as: 10.1002/ange.202111443

Link to VoR: https://doi.org/10.1002/ange.202111443

RESEARCH ARTICLE

Control of Hot Carrier Relaxation in $CsPbBr_3$ Nanocrystals Using Damping Ligands

Peng Zeng,[#a] Xinjian Ren,[#a] Linfeng Wei,[a] Haifeng Zhao,[a] Xiaochun Liu,[a] Xinyang Zhang,[a] Yanmin Xu,[b] Lihe Yan,[b] Klaus Boldt,[c] Trevor A. Smith,*[d] and Mingzhen Liu*[a]

[a] P. Zeng, X. Ren, L. Wei, X. Liu, X. Zhang, Prof. M. Liu
School of Materials and Energy, University of Electronic Science and Technology of China, Chengdu 611731, China
E-mail: mingzhen.liu@uestc.edu.cn
[b] Y. Xu, L. Yan
Key Laboratory of Physical Electronics and Devices of the Ministry of Education & Shaanxi Key Lab of Information Photonic Technique, School of Electronic Science and Engineering, Faculty of Electronic and Information Engineering, Xi'an Jiaotong University, Xi'an 710049, China
[c] K. Boldt
Department of Chemistry & Zukunftskolleg, University of Konstanz, 78457 Konstanz, Germany
[d] Prof. T. A. Smith
ARC Centre of Excellence in Exciton Science & School of Chemistry, The University of Melbourne, Parkville 3010, Victoria, Australia
E-mail: trevoras@unimelb.edu.au
# Authors contributed equally to this work.

Supporting information for this article is given via a link at the end of the document.

Abstract: In photon-conversion processes, rapid cooling of photo-induced hot carriers is a dominant energy loss channel. We herein report a 3-fold reduced hot carrier cooling rate in $CsPbBr_3$ nanocrystals capped with a cross-linked polysiloxane shell in comparison to single alkyl-chain oleylamine ligands. Relaxation of hot charge carriers depends on the carrier-phonon coupling (CPC) process as an important channel to dissipate energies in nanostructured perovskite materials. The CPC strengths in the two samples were measured through cryogenic photoluminescence spectroscopic measurements. The effect of organic ligands on the CPC in $CsPbBr_3$ nanocrystals is elucidated based on a damped oscillation model. This supplements the conventional polaron-based CPC model, by involving a damping effect on the CPC from the resistance of the ligands against nanocrystal lattice vibrations. The model also accounts for the observed linear temperature-dependence of the CPC strength. Our work enables predictions about the effect of the ligands on the performance of perovskite nanocrystals in future applications.

Introduction

Rapid cooling of photoinduced carriers with excess energy above the bandgap, or hot carriers (HCs), is one of the major energy loss channels in current photovoltaics applications.[1–3] These hot species rapidly relax to the band states commonly on a subpicosecond timescale. These processes are receiving intense interest following the triumph of the perovskite-based solar cells, in which photon-conversion efficiencies of up to 25% have been achieved in the last decade.[4] Therefore, by mitigating such hot energy losses and extracting the hot carriers before cooling, the possibility exists to enhance current photovoltaics device efficiencies beyond the Shockley-Queisser limit.[1,3,5] The emergence of all inorganic $CsPbX_3$ (X=I, Br, Cl) perovskite nanocrystals (PeNCs) have again revived the hot-carrier photovoltaics since the first successful synthesis of these materials.[6,7] $CsPbX_3$ NCs hold merits for applications in photovoltaics devices,[3,8] novel light-emitting materials such as light emitting diodes (LEDs)[9,10] and novel micro- and nanolasers.[11,12] Especially, it has been widely shown that $CsPbX_3$ NCs possess slow HC rates compared to common methylammonium (MA) or formamidinium (FA) based PeNCs, as a result of the inorganic cation Cs^+ suppressing the carrier-phonon coupling (CPC).[13–15] This is more favorable for maintaining a long time window for harvesting the excess energy from the hot electrons prior to being scattered by phonons, for which reason we herein focus on the $CsPbX_3$ NCs.[13,15,16]

Concurrently the underlying mechanisms of the hot carrier relaxation in both PeNCs and bulk perovskites are being unraveled.[3,17–20] It has been revealed that the relaxation is mostly mediated by the CPC interaction, in which hot carriers relax to band states mainly via emission of phonons.[2,17] One straightforward approach is to suppress CPC in order to reduce longitudinal optical (LO) phonon emission that will slow the HC cooling accordingly. Therefore understanding of the CPC in NCs is necessary in order to control the hot carrier cooling process. In the PeNC community, Iaru et al. discussed the Fröhlich interaction induced coupling of excitons and LO phonons in $CsPbBr_3$ NCs, and provided a measure for the strength of the Fröhlich interaction based on cryogenic photoluminescence (PL) spectra.[21] Saran et al. applied a Bose-Einstein two-oscillator model to interpret the interaction of electrons with acoustic and optical phonons.[22] Several groups have conducted cryogenic PL spectroscopic measurements on methylammonium- and Cs-based perovskite NCs, based on a universal thermal broadening model, in order to reveal the exciton dynamics including bonding energies, phonon modes and energies.[23–26] So far the PeNC community is still lacks an insightful investigation of a method for the direct control of the CPC and subsequently the HC cooling process. One may expect sizeor component-dependent CPC strengths, and indeed some works so far have revealed such a dependence in $CsPbX_3$ NCs.[13–16,18,27] However, size- and/or component-control is not feasible for applications that require specified optical properties of NCs and usually either size or component need to be maintained. By thinking outside the (particle-in-a-)box, surface ligands in the

NC system may provide a way by which the CPC can be tuned. A few studies have been conducted for conventional II-VI colloidal NCs such as CdSe and CdTe semiconductor quantum dot (QD) systems. Lifshitz et al.[28] and Weiss et al.[29] summarized the role of ligands in determining exciton relaxation dynamics in semiconductor QDs, respectively. Tisdale et al. further investigated the surface ligands on phonon properties with a mass-loading oscillator model.[30] Recently, Schnitzenbaumer and Dukovic observed different phonon damping behavior in CdTe QDs capped with organic and inorganic ligands.[31] These works have indicated a means to tailor the CPC by simple modulation of the surface ligands. However little work has realized control of the CPC using ligands in PeNCs. There remains challenges for PeNCs as unlike the CdSe and CdTe semiconductor QDs, especially the all inorganic PeNCs show more ionic properties.[32,33] Recently, Nie et al. found that using Cs_4PbBr_6 as the inorganic surface ligands provides an interfacial phonon dissipation channel which is able to effectively harness the CPC and thus the hot carrier relaxation dynamics in $CsPbBr_3$ NCs.[34] Manoli et al. reported a modulation effect on CPC by using different ligands.[35] There is still a lack of insight into the effects of commonly used organic ligands on the CPC in $CsPbX_3$ NCs; despite this being of universal significance in further practical applications. The underlying mechanism is even far less discussed.

We herein raise the question in what ways ligands affect the CPC interaction and subsequently the hot carrier relaxation. Based on our previous success in the synthesis of polysiloxane-wrapped $CsPbBr_3$ NCs,[36] we find a significantly slowed HC cooling process (more than 3-fold slower) in the polysiloxane-capped $CsPbBr_3$ NCs in comparison to conventional long alkyl chain oleylamine (OAm) ligands (OAm-$CsPbBr_3$), using ultrafast transient absorption spectroscopy. The former was capped with (3-aminopropyl)triethoxysilane (APTES) ligands which formed a thin polysiloxane wrapping layer. We attribute the retarded HC cooling process to the suppressed CPC process caused by the cross-linked APTES, and found evidence for the weak CPC strength in the APTES-$CsPbBr_3$ through cryogenic PL spectroscopy measurements. We modeled the ligand as a damper in an oscillation model that describes the electron-LO phonon coupling. The model predicts a mechanical damping effect on the CPC strength by the resistance of surface ligands against the lattice vibrations. Different capping ligands may possess different stiffness or rigidity that results in a varied damping effect. Our model also successfully rationalized the linear temperature dependence and the difference of CPC strength in two samples. Our work confirms the crucial role of the surface ligands in the CPC of perovskite NCs, and provides a way of controlling the HC cooling process. From a wider perspective, our fundamental understanding of the CPC will lead to both theoretical interest and practical inspiration to the perovskite community of future optoelectronic and photonic applications of the PeNCs.

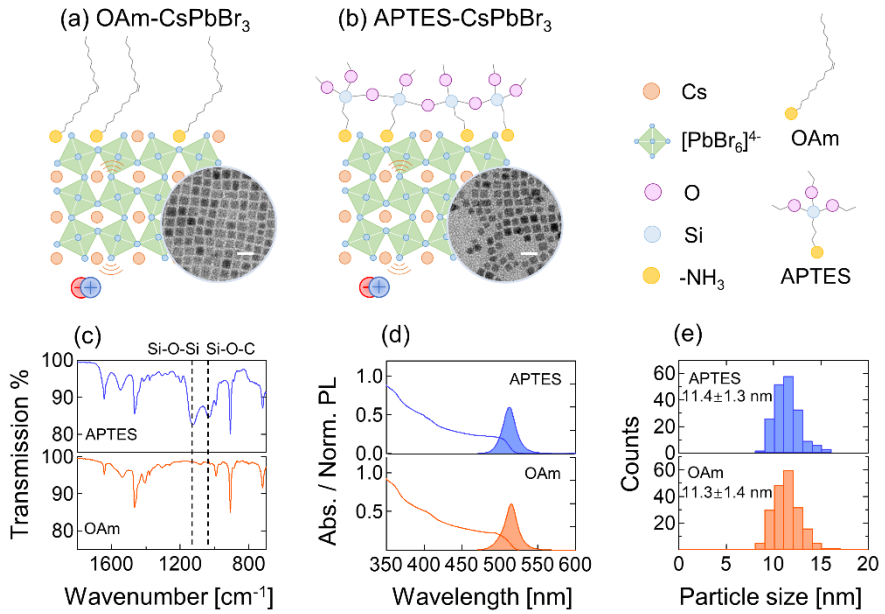

Figure 1. Schematic illustrations and TEM images of (a) OAm- and (b) APTES-$CsPbBr_3$ nanocrystals. (c) Fourier transform IR transmission and (d) UV-visible absorption spectra of samples. (e) Particle size distributions of OAm- and APTES-$CsPbBr_3$ nanocrystals from TEM measurements. OAm: oleylamine; APTES: (3-aminopropyl)triethoxysilane. Scale bars are 20 nm.

Results and Discussion

OAm- and APTES-$CsPbBr_3$ NCs were prepared according to our previous work.[36] Figure 1 shows schematic illustrations of $CsPbBr_3$ NCs with OAm and APTES surface ligands. OAm with a single alkyl chain is the commonly used surface ligand, in which the ammonium group interacts with Br^- ions at the perovskite lattice edge.[37] By replacing OAm with APTES as the precursor, our previous work has successfully realized monodisperse $CsPbBr_3$ NCs wrapped with a thin cross-linked polysiloxane layer via a control of the mutual hydrolysis process of the dangling

siloxane groups. Particularly, Fourier transform infrared (FTIR) spectroscopy measurements confirmed the presence of the Si-O-Si component (2870 cm^{-1}) in APTES-$CsPbBr_3$ NCs, indicative of the occurrence of the hydrolysis process and thus the formation of cross-linked molecules (see Figure 1c). Previous energy-dispersed X-ray spectroscopy measurements mapped the thin wrapping layer of polysiloxane around the particle.[36] Characterization indicated similar absorption and PL emission spectra for both samples as shown in Figure 1d. Herein particle sizes of the two samples were carefully controlled to be nearly identical, in order to eliminate the potential complication brought on by the size-dependence of the phonon coupling process. TEM images show the edge lengths are 11.3±1.4 nm and 11.4±1.3 nm for OAm and APTES-$CsPbBr_3$ NCs, respectively (see Figure 1e).

Femtosecond transient absorption (TA) spectroscopic measurements were subsequently carried out, in order to directly distinguish the HC cooling processes in the OAm- and APTES-$CsPbBr_3$ NC systems. The TA experimental layouts were based on previous works and details are also given in the SI.[38,39] 400 nm pump was employed to excite the NC ensemble in order to induce initial hot carrier populations. Figure 2 shows the transient spectral features at varying delay times after 400 nm excitation. The particles were excited under low pump fluence conditions, which delivered an average excitons per particle $\langle N \rangle$ is 0.2 with 6 nJ pulse energy (laser beam power 3 μW) thus alleviating issues relating to Auger process. (The average exciton density of 1×10^{17} cm^{-3} . See SI for details.) Details of the power-dependence of TA signals, calculation of exciton density and high power TA results are provided in Figure S4 and S5. What's worth mentioning is that there is no necessity to distinguish the respective contributions from electrons and holes to the TA signals, which are approximately equal due to their similar effective mass. The dominant bleaching peaks at around 500 nm are assigned to the band-edge transitions in both samples. The blue-side tail bands were caused by the population of hot electrons.[5,34] At the initial stage after photoexcitation, the carrier-phonon scattering effect rapidly results in a non-equilibrium hot electron distribution that follows the Fermi-Dirac distribution; we thus extracted the hot electron temperature, T_e by fitting the ΔOD using the equation:[19]

$$\Delta A^* = \left(1 - f_e(E, E_F, T_e)\right)^2 A_{\mathrm{ex}}\left(E; E_g - \Delta E_g\right) - A_0\left(E; E_g\right), \quad (1)$$

in which we reasonably assumed similar distributions for both the electrons and holes, and ΔA^* is the scaled change in absorption measured by transient absorption spectroscopy, f_e is the Fermi-Dirac distribution, E_F is the quasi-Fermi energy, T_e is the hot electron temperature, E_g is the bandgap energy with the energy shift ΔE_g, A_0 and A_{ex} are the absorption spectra before and after excitation, respectively. More details of the extraction of T_e from TA spectra are provided in the SI. We summarize and compare the T_e kinetics of both samples as plotted in Figure 2e, and fit a bi-exponential function to the T_e decays. The APTES-$CsPbBr_3$ exhibits a distinctly slower decay of the hot electron temperature down to below 400 K (740 fs), compared to the OAm-$CsPbBr_3$ NC system (220 fs). Our results are in close accord with reported HC cooling times in most perovskite materials.[2]

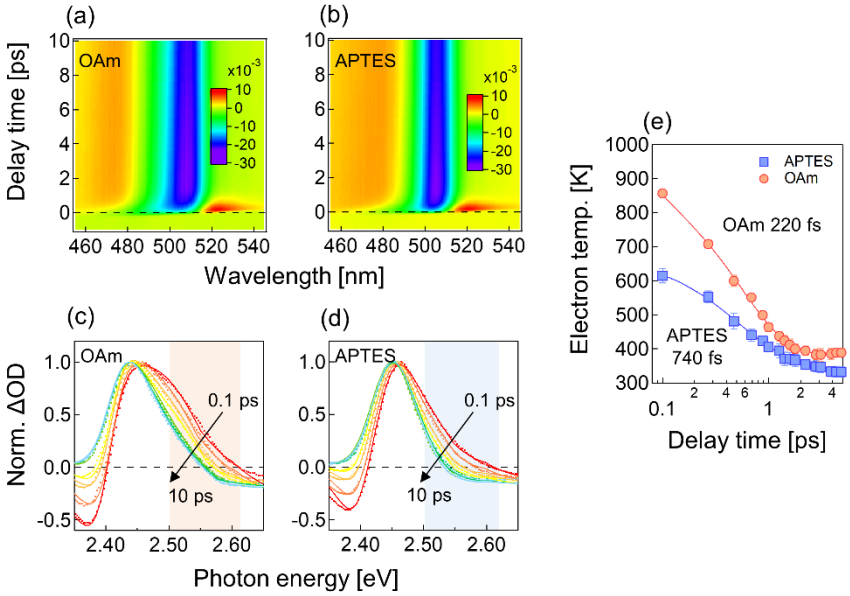

Figure 2. Pseudocolor maps of TA spectra for (a) OAm- and (b) APTES-$CsPbBr_3$ NCs measured at room temperature, upon excitation at 400 nm. The chirp of the probe pulses was corrected by a cross-correlation analysis of the initial TA rising signals. Normalized TA spectral slices of (c) OAm- and (d) APTES-$CsPbBr_3$ NCs at delay times from 0.1 to 10 ps. Dots are measured results and lines are from the Fermi-Dirac distribution fittings. The shadow regions indicate the blue-side tail-like bands. (e) Hot electron temperature T_e decay for OAm- (orange circles) and APTES-$CsPbBr_3$ (blue squares) NCs. Error bars are from the fitting procedure. The solid lines are from exponential decay fittings of the electron temperature.

It should be noted that HC cooling is susceptible to the photoinduced carrier density. We additionally excited the samples with a high photon flux of 60 nJ pulse energy (laser beam power 30 μW), as shown in Figure S5, resulting in a $\langle N \rangle$ of 0.7 corresponding to an average carrier density over 6×10^{17} cm^{-3}. In Figure S6, the derived HC temperature decay processes for both samples exhibited an initially high HC temperature and prolonged two-stage-like cooling process in line with most reported

work.[13,34] The retarded two cooling stages are ascribed to hot-phonon bottleneck and Auger-heating effects, respectively.[2,13] The former involves a fast accumulation of a hot LO phonon population that reduces the phonon-assisted HC cooling efficiency, whereas the latter results in re-excitation of band-gap carriers, which leads to a dynamical long-time population of hot carriers. In comparison to the high density condition, our low excitation pump ensured the absence of either hot phonon or Auger effects, allowing solitary analysis of the CPC-assisted HC cooling process in the $CsPbBr_3$ system. Notably, APTES-capped $CsPbBr_3$ still possesses a slower HC cooling rate than OAm-$CsPbBr_3$ NCs with initial high carrier density. It should be noted that the trapping effect at the interface could cause modification of HC cooling through capturing carriers into surface defect states, The observed fast relaxation could be the coupling to surface related defect/trap sates.[40-42] In our case, these two samples exhibited similar PLQYs above 50%, indicating similar surface vacancy densities in both systems. In addition, as shown in Figure S11, the band-edge TA bleaches for both complexations show closely matched rising and initial decaying kinetics at the initial stage, during which the fast surface trapping usually happens.[43, 44] Therefore, the surface defects show negligible effect in the HC cooling.

These results indicate an important role the surface ligands play in the HC cooling process in $CsPbBr_3$ NCs. Previous studies excluded the energy transfer to ligands from hot electrons as the major relaxation channel in $CsPbX_3$ NCs,[45] as the organic ligands possess nontrivial absorption cross sections at the energy of phonons. A more likely mechanism is the modulation effect upon the CPC interaction by surface ligands. Different ligands may impinge CPC via different surface electrostatic environment parameters such as dipoles and dielectric constants. As in our case, $CsPbBr_3$ NCs were large particles of over 10 nm edge length, thus under a weak quantum confinement condition.[46] The surface ligands therefore exhibit only a limited outer-dielectric medium induced effect on the CPC. A recent study compared the HC cooling in $CsPbBr_3$ NCs capped with single molecule ZI (3-*N*,*N*-(dimethyloctadecylammonio)propansulfonate) and DDAB (didodecylammonium bromide) ligands respectively.[17] The former is a long chain zwitterion and the latter a symmetric didodecylammonium molecule, thus the two ligand species possess significantly different dipole moments. Identical cooling dynamics were found in the two samples, which suggests a negligible electro-effect upon the CPC. A mechanical effect should be taken into account in our case. The use of cross-linked polysiloxane shell ligands may introduce a remarkable stiffness against the particle surface, whereas the mono-dispersed OAm ligands are more flexible. Indeed, the mechanical effect of surface ligands on phonon properties was modeled as a mass-loading oscillator in a CdSe NC system by Tisdale and coworkers.[30] Notably, the ligand surface density may also impact the CPC process. Based on our sythesis process, similar ligand densities were found to be 8.71 nm^{-2} and 8.10 nm^{-2} for APTES-$CsPbBr_3$ and OAm-$CsPbBr_3$, respectively (see Figure S7). Thus ligand density effect can be excluded in this work.

In order to investigate the possible role for the surface ligands in CPC, we herein reiterate the CPC and its associated PL emission process. Generally, in perovskite materials, carriers and LO phonons are coupled as a form of polarons, i.e., charge carriers dressed by the local lattice polarization resulting from the Coulomb interaction between the carrier and the ionic lattice.[47] Previous studies have revealed the dependence of the CPC strength onthe material dielectric constants based on the Feynman polaron model.[48] For $CsPbBr_3$ a typical ionic material, we take the electron as an example given the similar effective mass of electrons and holes; the CPC strength S follows:

$$S = \frac{e^2}{\hbar c}\sqrt{\frac{m^* c}{2\hbar\omega_{\mathrm{LO}}}}\left(\frac{1}{\epsilon_\infty}-\frac{1}{\epsilon_0}\right), \qquad (2)$$

where m^* is the effective mass of the electron, ϵ_∞ and ϵ_0 are the high-frequency and static dielectric constants of $CsPbBr_3$, respectively, and the overall dielectric term represents the ionic screening of electrons. From a phonon emission perspective, S also indicates the possibility for the generation of a single phonon via the CPC process. Upon photoexcitation of the NCs, the hot carriers with excess energy interact with the crystal lattice, via the electrostatic interaction between the dipole of the charge carrier and the lattice oscillations. The latter then results in emission of phonons, in which LO modes usually involve higher energies than others such as acoustic modes. Subsequently, the phonon-assisted radiative exciton recombination results in emitted photons with the one (or multiple) phonon-energy lower than the zero-phonon band (ZPB). Therefore, the electron-LO phonon coupling strength, S can be quantized through refined PL spectra. In particular, the *n*th-order LO phonon intensity distribution I_n In follows a Poisson distribution $I_n = I_0 S^n/n!$, where n is the number of phonons involved in the coupling process (see SI for details). Meanwhile, the intensity of the PL sideband should be equal to the appropriate phonon numbers. As a result, the PL emission intensity ratio between the 1st order LO phonon-assisted and the ZPB emission yields the LO-phonon coupling strength S.[49,50] It has been pointed out that the influence of exciton energy distribution, or the particle size distribution effect can be excluded using the PL emission peak intensity ratios. It may lead to an artificial dependence of the electron-phonon coupling strength on experimental conditions if wavelength-integrated PL intensities are applied.[50]

Cryogenic PL spectroscopic measurements, which are able to eliminate PL broadening caused by thermal electron energies, were carried out in order to directly observe LO replicas. NCs dispersed in octane were first dropped on a glass substrate and solvents were then naturally evaporated. Figure 3a and b show comparison of the PL spectra at 4.8 K and 300 K for both samples, respectively. The room temperature PL spectrum is quite symmetric whereas the cryogenic PL exhibits an obviously asymmetric profile with a sidebandat lower energies in both NCs. The low-energy sideband becomes less significant when the temperature is elevated, and the two peaks are almost merged into a single Gaussian peak at 50 K and above as indicated by Figure 3c and d. We applied a two-Gaussian peak fitting procedure (for an ensemble of nanoparticles, PL may be fitted with the Gaussian profile as for the size distribution) to the PL spectra measured from 4.8 to 50 K. Figure 3e shows a similar energy separation of about 15 meV between the ZPB (higher energy) and the sideband (lower energy) peaks, for both OAm- and APTES-$CsPbBr_3$ NCs, which agrees with the reported Raman spectroscopy measured LO phonon energy of 16 meV[51] and 18 meV[52] in $CsPbBr_3$. We therefore suggest that the sideband PL emission originates from the 1st order LO phonon-assisted exciton recombination.

The temperature-dependent CPC strength of OAm- and APTES-capped $CsPbBr_3$ NCs are compared from 4.8 to 50 K in Figure 3f. All the cryogenic PL measurements were repeated twice from independent sample batches in order to ensure the reproducibility (see Figure S3). Detailed analysis of the cryogenic PL spectra is given in Figure S1 and S2. The APTES-$CsPbBr_3$ system shows a significantly weaker CPC strength compared with the OAm system. We therefore suggest that a weaker CPC process is observed in the APTES-capped $CsPbBr_3$ NCs. Additionally, analysis of temperature-dependent PL broadening above 60 K also reveals a weaker LO phonon coupling effect in the APTES-$CsPbBr_3$ NCs than in OAm-capped NCs. The PL spectral broadening of an NC ensemble is composed of intrinsic broadening (Γ_{intr}), exciton-acoustic phonon broadening ($\Gamma_{\mathrm{AP}}T$), and exciton-LO phonon broadening that follows a Boltzmann thermal distribution ($\Gamma_{\mathrm{LO}}/(\exp(\hbar\omega_{\mathrm{LO}}/kT)-1)$).[53] As shown in Figure 3g, the temperature dependent PL broadening thus indicates a notably lower contribution of Γ_{LO}=31 meV from the LO-phonon interaction to the PL emission line broadening in the APTES-$CsPbBr_3$ NCs, compared to that of Γ_{LO}=60 meV in OAm-$CsPbBr_3$. Our results are in line with most reported LO-phonon induced broadening Γ_{LO} ranging from 27 to 86.7 meV in $CsPbBr_3$ NCs.[22–24,26]

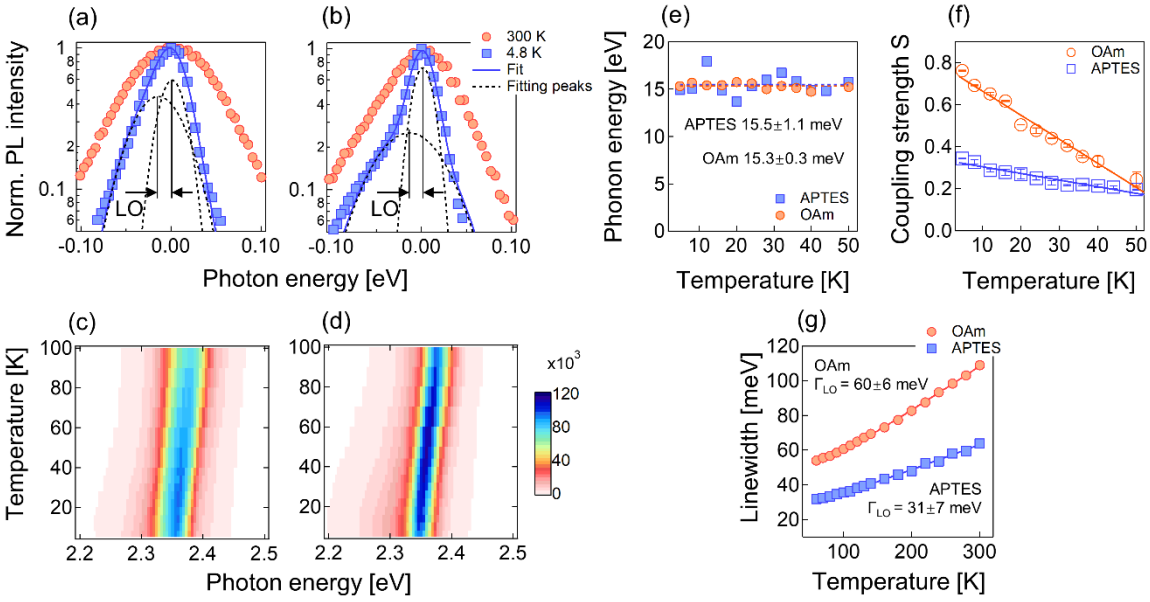

Figure 3. PL emission spectra of (a) OAm- and (b) APTES-$CsPbBr_3$ NCs measured at 4.8 K (blue squares) and 300 K (orange circles), upon excitation at 405 nm. Spectra at different temperature are shifted to center at the emission peak for clear comparison. Blue solid lines are the fitted spectra from a two-Gaussian peak model; and the dashed lines represent the individual fitting peaks. Note that the PL intensity axis is logarithmic. Pseudocolor maps of temperature-dependent PL spectra of (c) OAm- and (d) APTES-$CsPbBr_3$ NCs from 4.8 K to 100 K. (e) Phonon energies derived from the peak fitting to the PL emission spectra at different temperature for OAm- (orange circles) and APTES-capped (blue squares) $CsPbBr_3$ NCs. Dashed line represents the average phonon energies. (f) Derived carrier-LO phonon coupling strength as a function of temperature ranging from 4.8 K to 50 K, for OAm- (orange circles) and APTES-$CsPbBr_3$ (blue squares) NCs. The solid lines represent linear fittings to the temperature-dependence of the coupling strength. Error bars are from independent measurements and analysis of two batches of samples. (g) Temperature-dependence of PL emission spectral width (FWHM) of OAm- (orange circles) and APTES-$CsPbBr_3$ (blue squares) NCs from 60 K to 300 K. Solid lines are the fitting results based on the PL broadening model.

Interestingly, the CPC strength for both systems decreases linearly with increasing temperature. In particular the APTES-$CsPbBr_3$ exhibits a smaller slope than the OAm-$CsPbBr_3$. Lao et al. also reported a similar linear decreasing dependence of the CPC strength in a $CsPbBr_3$ nanosheet system.[52] Based on the polaron-based CPC model given by Eqn. 2, we hypothesize that the observed temperature dependence of the coupling strength originates from the temperature-dependent static dielectric constant ϵ_0, as the high-frequency dielectric constant has been shown to be independent on temperature in the $CsPbBr_3$ material.[54] However, the relation does not predict the observed difference in the temperature-dependence of the CPC strength between the two samples, as phonon energies, ω_{LO}, are found to be almost identical in the two systems.

The above observations raise questions relating to the origin of the difference in CPC strengths and their linear temperature-dependence. The latter is easy to understand; given the observed linear-like dependence of S on temperature, the static dielectric constant, ϵ_0 must be inversely proportional to temperature in order to conform to the linear decay. Indeed, extensive studies have identified the reciprocal proportion relation of the static dielectric constant against cryogenic temperature, namely $\epsilon_0 = T/c_T$ where c_T reflects the dielectric properties of $CsPbBr_3$, or the Curie-Weiss law in cubic ionic compounds.[55–57] On the contrary, although no works so far have reported observation of the Curie-Weiss relationship in $CsPbBr_3$, our finding may provide indirect evidence for the reciprocal proportion relation of the ϵ_0 upon temperature.

We continue to investigate the mechanical effect of surface ligands on phonon properties, by employing a damped oscillator model with the frequency, ω_{LO} of the LO phonon mode. The ligand applies a resistance against the motion of the oscillation as schematically illustrated in Figure 4a. The electron at the opposite end triggers the oscillation at time $t = 0$. Hence, an underdamped oscillation is given by:

$$x(t) = x_0 \exp(-\zeta\omega_{LO}t)\cos(\omega_d t), \quad (3)$$

in which the amplitude $x(t)$ reflects the amplitude of the phonon, which thus yields thetime dependence of the CPC strength. Consequently, the coupling strength between the electron and the phonon is modulated by a dimensionless damping ratio ζ, which describes the resistance of the surface ligand layer against the lattice vibrations. In comparison to the non-damped condition given $x(t) = x_0\cos(\omega_0 t)$, the oscillation is damped with a damping factor of $\exp(-\zeta\omega_{LO}t)$. The frequency of the damped oscillation, ω_d is modulated to be $\omega_{LO}\sqrt{1-\zeta^2}$. Schnitzenbaumer et al. showed an LO phonon-under-damped process by organic surface ligands in CdSe NC systems.[31] Similarly, we herein assume a weak damping condition with $\zeta \ll 1$. Integration of the damping factor over time, $\int \exp(-\zeta\omega_{LO}t)\,dt$, yields the overall coupling strength $\bar{S} \propto \zeta^{-1}S$. As the phonon dissipates faster due to an increased damping ratio attributed to a more rigid ligand shell, the efficiency with which energy is transferred to the lattice via CPC is reduced.

The damped coupling strength is given as follow according to Eqn. 2:

$$\bar{S} = \frac{1}{\zeta\epsilon_\infty} - \frac{1}{c_T\zeta}. \quad (4)$$

Obviously, the slope of the temperature-dependence is determined by the damping ratio, ζ, of the surface ligands. By comparison to the single alkyl chain of OAm, the APTES ligands possess a remarkable stiffness as a result of the cross-linked polysiloxane shell. Using density functional theory, we calculated and compared the molecular energies of the ligands at different geometry configurations (see Figure S8 in SI). The cross-linked APTES dimmer is obviously more difficult to fold up in comparison to the OAm molecules. It is rational to consider a stronger damping effect of the APTES ligands on the lattice vibrations, most likely $\zeta_{APTES} > \zeta_{OAm}$. Evidently, the APTES-$CsPbBr_3$ NC system shows a less steep decay of the CPC strength with increasing temperature. This is strikingly consistent with the observed linear dependence for both samples. It further rationalizes our interpretation of the damping effects of surface ligands on the CPC strength. Consistently, the APTES-$CsPbBr_3$ NC species exhibited a slowed hot carrier cooling process as a result of the suppressed CPC process, as illustrated in Figure 4.

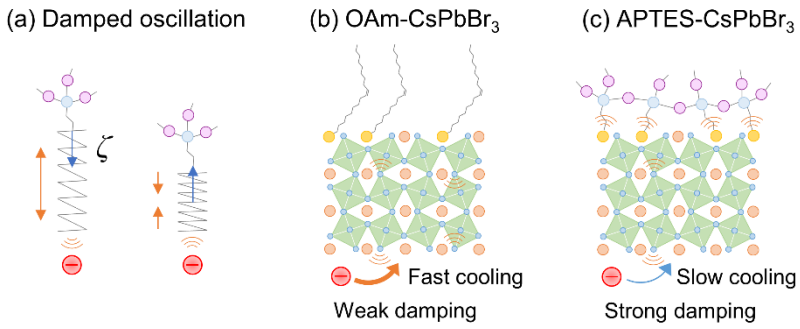

Figure 4. Schematic illustrations of (a) damped oscillation model and ligand effect on hot carrier cooling process in (b) OAm- and (c) APTES-capped $CsPbBr_3$ NCs.

The damped oscillation model semi-quantitatively rationalizes the effects of surface ligands in the CPC process, and more importantly, allows interpretation of the linear temperature-dependent CPC strength. However, there still remain a few concerns. One is on the quantitative and descriptive model of the damping effect of surface ligands. We expect multiple factors that impact the damping effect, including the strength of chemical bonds, molecular weights, and molecular stiffness or rigidity. Additionally, we introduced an aromatic-ligand capped $CsPbBr_3$ system based on our previous well-developed synthesis method as a supplement to our coupling model. The aromatic ligands were 1-naphthoic acid (NCA) instead of oleic acid through a post-synthesis ligand-exchange strategy, based on our very recent work,[58] as shown in Figure S12. By applying the cryogenic PL measurements and emission line-width analysis, we found a moderate phonon coupling strength for NCA-$CsPbBr_3$, between that of OAm- and APTES-capped $CsPbBr_3$ NCs, as shown in Figure S13. This is in line with the expectation of the rigidity or the loading of the anchored aromatic rings, which exhibit less rigidity but more significant resistance than the cross-linked APTES and the alkyl chain OAm, respectively.

Vibrations of ligands may play a role in exciton energy dissipation processes, which may further complicate the damped oscillation model with their intrinsic vibrations. We herein excluded the effects of the vibrational modes of the ligands themselves on the damping, because the ligand molecules usually possess a few orders of magnitude (1000 cm^{-1}) higher vibrational frequency than the phonons in $CsPbBr_3$ NCs (100 cm^{-1}).

Another concern regards the ligand density at the particle surfaces as mentioned above. Besides carefully control the identical ligand density in the two systems, we also show that more ligands introduce a weaker phonon-coupling effect in the OAm-capped $CsPbBr_3$ NCs, by applying washing agents of different volumes as shown in Figure S14.

Thus high ligand density and ligand shells with more significant resistance against lattice vibrations, may be favorable to slowing down the carrier relaxation process. However, the charge transfer efficiency may be affected by the introduction of such highly resistant but insulating ligands at the particle surfaces.[59,60] We suggest that rational design of ligand molecules will be able to boost charge carrier delocalization and thus enhance the transfer efficiency, while simultaneously leading to significant damping effects, in favor of hot carrier harvest.

Conclusion

In conclusion, we revealed the damping effect of surface ligands on the phonon coupling process in $CsPbBr_3$ NCs through analysis of cryogenic PL spectroscopic measurements, and successfully suppressed the rapid HC cooling rate using damping ligands. APTES ligands provide a more significant damping effect leading to the suppressed CPC strength, compared to the conventional single-alkyl-chain OAm ligands. More interestingly, both samples show a linear decay dependence of the CPC strength with increasing cryogenic temperature; the APTES results in a more suppressed decaying coupling strength. We then rationalized the different coupling strength and its different temperature-dependence between samples, by establishing a ligand-damping model of the CPC process. Ultrafast TA spectroscopy measurements revealed a longer hot electron lifetime in the APTES-$CsPbBr_3$ NC system, thus confirming the suppressed coupling effect from the damping effect of APTES ligands. Our work provides a way of controlling the CPC process in the perovskite NCs via engineering of the surface ligands. This may lay fundamentals for further development of optoelectronic and photonic applications of the perovskite nanostructures.

Acknowledgements

This work was supported by the National Key R&D Program of China (2017YFA0207400), the National Natural Science Foundation of China (61905037 and 62104027), the Special Program for Sichuan Youth Science and Technology Innovation Research Team (2019JDTD0006), and the Fundamental Research Funds for the Central Universities of China (ZYGX2019J028). K. B. acknowledges support by the Zukunftskolleg Konstanz through a 5-Year Research Fellowship. T. A. S. acknowledges support by the Australian Research Council Centre of Excellence in Exciton Science (CE170100026).

Keywords: cryogenic photoluminescence • $CsPbBr_3$ nanocrystals • hot charge carriers • transient absorption • phonon coupling

Author Contributions: P. Z. and X. R. contributed equally to this work. P. Z., T. A. S. and M. L. conceived the whole project. X. R., X. L., L. W., H. Z. and X. Z. synthesized and characterized the $CsPbBr_3$ NCs. P. Z. and X. R. designed and performed the cryogenic PL measurements. P. Z., X. R., T. A. S., X. L., Y. X. and L. Y. designed and performed the TA measurements. P. Z., T. A. S., K. B. and M. L. were responsible for the fundamental model of the CPC interaction, and performed data analysis with X. R. All authors have given approval to the final version of this manuscript.

[1] R. T. Ross, A. J. Nozik, *J. Appl. Phys.* **1982**, *53*, 3813–3818.
[2] M. Li, J. Fu, Q. Xu, T. C. Sum, *Adv. Mater.* **2019**, *31*, 1802486.
[3] M. Li, S. Bhaumik, T. W. Goh, M. S. Kumar, N. Yantara, M. Grätzel, S. Mhaisalkar, N. Mathews, T. C. Sum, *Nat. Commun.* **2017**, *8*, 14350.
[4] G. Kim, H. Min, K. S. Lee, D. Y. Lee, S. M. Yoon, S. I. Seok, *Science* **2020**, *370*, 108–112.
[5] B. T. Diroll, R. D. Schaller, *Adv. Funct. Mater.* **2019**, *29*, 1901725.
[6] L. Protesescu, S. Yakunin, M. I. Bodnarchuk, F. Krieg, R. Caputo, C. H. Hendon, R. X. Yang, A. Walsh, M. V. Kovalenko, *Nano Lett.* **2015**, *15*, 3692–3696.
[7] M. V. Kovalenko, L. Protesescu, M. I. Bodnarchuk, *Science* **2017**, *358*, 745–750.
[8] H. Bian, D. Bai, Z. Jin, K. Wang, L. Liang, H. Wang, J. Zhang, Q. Wang, S. F. Liu, *Joule* **2018**, *2*, 1500–1510.
[9] G. Li, F. W. R. Rivarola, N. J. Davis, S. Bai, T. C. Jellicoe, F. de la Peña, S. Hou, C. Ducati, F. Gao, R. H. Friend, N. C. Greenham, Z. K. Tan, *Adv. Mater.* **2016**, *28*, 3528–3534.
[10] A. Swarnkar, R. Chulliyil, V. K. Ravi, M. Irfanullah, A. Chowdhury, A. Nag, *Angew. Chem. Int. Ed.* **2015**, *54*, 15424–15428.
[11] Y. Wang, X. Li, J. Song, L. Xiao, H. Zeng, H. Sun, *Adv. Mater.* **2015**, *27*, 7101–7108.
[12] Q. Wei, X. Li, C. Liang, Z. Zhang, J. Guo, G. Hong, G. Xing, W. Huang, *Adv. Opt. Mater.* **2019**, *7*, 1900080.
[13] J. Chen, M. E. Messing, K. Zheng, T. Pullerits, *J. Am. Chem. Soc.* **2019**, *141*, 3532–3540.
[14] S. Masada, T. Yamada, H. Tahara, H. Hirori, M. Saruyama, T. Kawawaki, R. Sato, T. Teranishi, Y. Kanemitsu, *Nano Lett.* **2020**, *20*, 4022–4028.
[15] T. R. Hopper, A. Gorodetsky, A. Jeong, F. Krieg, M. I. Bodnarchuk, M. Maimaris, M. Chaplain, T. J. Macdonald, X. Huang, R. Lovrincic, M. V. Kovalenko, A. A. Bakulin, *Nano Lett.* **2020**, *20*, 2271–2278.
[16] T. R. Hopper, A. Gorodetsky, J. M. Frost, C. Müller, R. Lovrincic, A. A. Bakulin, *ACS Energy Lett.* **2018**, *3*, 2199–2205.
[17] J. Fu, Q. Xu, G. Han, B. Wu, C. H. A. Huan, L. M. Lee, T. C. Sum, *Nat. Commun.* **2017**, *8*, 1300.
[18] T. Wang, L. Jin, J. Hidalgo, W. Chu, J. M. Snaider, S. Deng, T. Zhu, B. Lai, O. Prezhdo, J. P. Correa-Baena, L. Huang, *Sci. Adv.* **2020**, *6*, eabb1336.
[19] J. W. M. Lim, D. Giovanni, M. Righetto, M. Feng, S. G. Mhaisalkar, N. Mathews, T. C. Sum, *J. Phys. Chem. Lett.* **2020**, *11*, 2743–2750.
[20] Z. Guo, Y. Wan, M. Yang, J. Snaider, K. Zhu, L. Huang, *Science* **2017**, *356*, 59–62.
[21] C. M. Iaru, J. J. Geuchies, P. M. Koenraad, D. Vanmaekelbergh, A. Y. Silov, *ACS Nano* **2017**, *11*, 11024–11030.
[22] R. Saran, A. Heuerjungemann, A. G. Kanaras, R. J. Curry, *Adv. Opt. Mater.* **2017**, *5*, 1700231.
[23] J. Ramade, L. M. Andriambariarijaona, V. Steinmetz, N. Goubet, L. Legrand, T. Barisien, F. Bernardot, C. Testelin, E. Lhuillier, A. Bramati, M. Chamarro, *Appl. Phys. Lett.* **2018**, *112*, 072104.
[24] Q. Han, W. Wu, W. Liu, Q. Yang, Y. Yang, *J. Lumin.* **2018**, *198*, 350–356.
[25] B. Ai, C. Liu, Z. Deng, J. Wang, J. Han, X. Zhao, *Phys. Chem. Chem. Phys.* **2017**, *19*, 17349–17355.
[26] B. T. Diroll, H. Zhou, R. D. Schaller, *Adv. Funct. Mater.* **2018**, *28*, 1800945.
[27] P. Ijaz, M. Imran, M. M. Soares, H. Tolentino, B. Martingarcia, C. Giannini, I. Moreels, L. Manna, R. Krahne, *J. Phys. Chem. Lett.* **2020**, *11*, 2079–2085.
[28] E. Lifshitz, *J. Phys. Chem. Lett.* **2015**, *6*, 4336–4347.
[29] M. D. Peterson, L. C. Cass, R. D. Harris, K. Edme, K. Sung, E. A. Weiss, *Annu. Rev. Phys. Chem.* **2014**, *65*, 317–339.
[30] E. Lee, A. J. Mork, A. P. Willard, W. A. Tisdale, *J. Chem. Phys.* **2017**, *147*, 044711.
[31] K. J. Schnitzenbaumer, G. Dukovic, *Nano Lett.* **2018**, *18*, 3667–3674.
[32] H. Huang, M. I. Bodnarchuk, S. V. Kershaw, M. V. Kovalenko, A. L. Rogach, *ACS Energy Lett.* **2017**, *2*, 2071–2083.
[33] A. Pan, B. He, X. Fan, Z. Liu, J. J. Urban, A. P. Alivisatos, L. He, Y. Liu, *ACS Nano* **2016**, *10*, 7943–7954.

[34] Z. Nie, X. Gao, Y. Ren, S. Xia, Y. Wang, Y. Shi, J. Zhao, Y. Wang, *Nano Lett.* **2020**, *20*, 4610–4617.
[35] A. Manoli, P. Papagiorgis, M. Sergides, C. Bernasconi, M. Athanasiou, S. Pozov, S. A. Choulis, M. I. Bodnarchuk, M. V. Kovalenko, A. Othonos, G. Itskos, *ACS Appl. Nano Mater.* **2021**, *4*, 5084-5097.
[36] H. Zhao, L. Wei, P. Zeng, M. Liu, *J. Mater. Chem. C* **2019**, *7*, 9813–9819.
[37] J. Song, T. Fang, J. Li, L. Xu, F. Zhang, B. Han, Q. Shan, H. Zeng, *Adv. Mater.* **2018**, *30*, 1805409.
[38] Y. Xu, L. Yan, J. Si, M. Li, Y. Ma, J. Li, X. Hou, *Carbon* **2020**, *165*, 421–427.
[39] J. Li, Z. Liang, X. Li, H. Li, Y. Wang, J. Qin, J. Tong, L. Yan, X. Bao, Y. Xia, *ACS Appl. Mater. Interfaces* **2020**, *12*, 8475–8484.
[40] M. Li, S. Bhaumik, T. W. Goh, M. S. Kumar, N. Yantara, M. Grätzel, S. Mhaisalkar, N. Mathews, T. C. Sum, *Nature Commun.* **2017**, *8*, 14350.
[41] S. V. Kilina, D. S. Kilin, O. V. Prezhdo, *ACS Nano* **2009**, *3*, 93-99.
[42] J. Chen, M. E. Messing, K. Zheng, T. Pullerits, *J. Am. Chem. Soc.* **2019**, *141*, 3532-3540.
[43] Q. Y. Li, T. Q. Lian, *J. Phys. Chem. Lett.* **2019**, *10*, 566-573.
[44] K. Wu, G. Liang, Q. Shang, Y. Ren, D. Kong, T. Lian, *J. Am. Chem. Soc.* **2015**, *137*, 12792-12795.
[45] Y. Li, R. Lai, X. Luo, X. Liu, T. Ding, X. Lu, K. Wu, *Chem. Sci.* **2019**, *10*, 5983–5989.
[46] J. Butkus, P. Vashishtha, K. Chen, J. K. Gallaher, S. K. K. Prasad, D. Z. Metin, G. Laufersky, N. Gaston, J. E. Halpert, J. M. Hodgkiss, *Chem. Mater.* **2017**, *29*, 3644–3652.
[47] M. Baranowski, P. Plochocka, *Adv. Energy Mater.* **2020**, *10*, 1903659.
[48] J. A. Steele, P. Puech, B. Monserrat, B. Wu, R. X. Yang, T. Kirchartz, H. Yuan, G. Fleury, D. Giovanni, E. Fron, M. Keshavarz, E. Debroye, G. Zhou, T. C. Sum, A. Walsh, J. Hofkens, M. B. J. Roeffaers, *ACS Energy Lett.* **2019**, *4*, 2205–2212.
[49] R. Heitz, I. Mukhametzhanov, O. Stier, A. Madhukar, D. Bimberg, *Phys. Rev. Lett.* **1999**, *83*, 4654–4657.
[50] H. Zhao, H. Kalt, *Phys. Rev. B* **2003**, *68*, 125309.
[51] C. C. Stoumpos, C. D. Malliakas, J. A. Peters, Z. Liu, M. Sebastian, J. Im, T. C. Chasapis, A. C. Wibowo, D. Y. Chung, A. J. Freeman, B. W. Wessels, M. G. Kanatzidis, *Cryst. Growth Des.* **2013**, *13*, 2722–2727.
[52] X. Lao, Z. Yang, Z. Su, Y. Bao, J. Zhang, X. Wang, X. Cui, M. Wang, X. Yao, S. Xu, *J. Phys. Chem. C* **2019**, *123*, 5128–5135.
[53] F. Zhang, H. Zhong, C. Chen, X. Wu, X. Hu, H. Huang, J. Han, B. Zou, Y. Dong, *ACS Nano* **2015**, *9*, 4533–4542.
[54] S. Govinda, B. P. Kore, M. Bokdam, P. Mahale, A. Kumar, S. Pal, B. Bhattacharyya, J. Lahnsteiner, G. Kresse, C. Franchini, A. Pandey, D. D. Sarma, *J. Phys. Chem. Lett.* **2017**, *8*, 4113–4121.
[55] A. J. Bosman, E. E. Havinga, *Phys. Rev.* **1963**, *129*, 1593-1600.
[56] G. Rupprecht, R. O. Bell, *Phys. Rev.* **1964**, *135*, A748-A752.
[57] Z. Wu, C. Ji, L. Li, J. Kong, Z. Sun, S. Zhao, S. Wang, M. Hong, J. Luo, *Angew. Chem. Int. Ed.* **2018**, *57*, 8140–8143.
[58] X. Liu, H. Zhao, L. Wei, X. Ren, X. Zhang, F. Li, P. Zeng, M. Liu, *Nanophotonics* **2020**, *10*, 1967-1975.
[59] E. T. Vickers, E. E. Enlow, W. G. Delmas, A. C. Dibenedetto, A. H. Chowdhury, B. Bahrami, B. W. Dreskin, T. A. Graham, I. N. Hernandez, S. A. Carter, S. Ghosh, Q. Qiao, J. Z. Zhang, *ACS Energy Lett.* **2020**, *5*, 817–825.
[60] J. Li, L. Xu, T. Wang, J. Song, J. Chen, J. Xue, Y. Dong, B. Cai, Q. Shan, B. Han, H. Zeng, *Adv. Mater.* **2017**, *29*, 1603885.

Entry for the Table of Contents

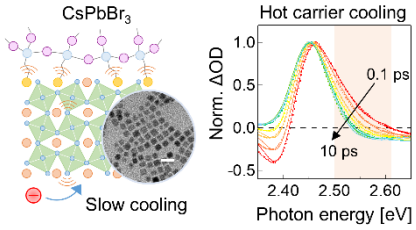

A model for the damping of the carrier-phonon coupling in all-inorganic perovskite nanocrystals (PeNCs) was proposed by considering the mechanical resistance of the ligands. Correspondingly the hot carrier cooling process was slowed down by 3-fold in $CsPbBr_3$ PeNCs by tuning the rigidity of the layer of organic capping ligands.